RSC Advances

ROYAL SOCIETY OF CHEMISTRY

www.rsc.org/advances

Cite this: DOI: 10.1039/c0xx00000x

www.rsc.org/xxxxxx

FULL PAPER

Inkjet-printed PEDOT:PSS electrodes on plasma-modified PDMS nanocomposites: quantifying plasma treatment hardness

Alessandro Chiolerio[a], Paola Rivolo[b], Samuele Porro[a], Stefano Stassi[a,b], Serena Ricciardi[b], Pietro Mandracci[b], Giancarlo Canavese[a], Katarzyna Bejtka[a] and Candido Fabrizio Pirri[a,b]

Received (in XXX, XXX) Xth XXXXXXXXX 20XX, Accepted Xth XXXXXXXXX 20XX
DOI: 10.1039/b000000x

Nanostructured polymeric composites are promising for the fabrication of piezoresistive devices, as they show a huge variation of the electrical resistance when subjected to a mechanical deformation. Quantum Tunneling Composites feature a conduction mechanism occurring between the metallic filler, copper particles, embedded in a polydimethylsiloxane (PDMS) insulating matrix, mechanism enhanced by the spiky morphology of the particles. PEDOT:PSS electrodes are patterned on either sides of the composite by means of inkjet printing, a technology which allows one-step fabrication processes. The adhesion and spreading of conductive printed ink drops are controlled and enhanced by pre-treating the samples surfaces in atmospheric pressure plasma customized system. Due to an extremely high metal to polymer ratio, resulting in different surface and dielectric properties of the composite, known plasma conditions are not suitable to allow control of the spreading. The optimal plasma conditions for the ink/surface compatibility are found using a quantitative comparison, based on image analysis and numerical interpretation of adhesion / roughness properties, such as bulging and spread.

Introduction

Tactile sensing technology can be defined as the ability to transduce a given property of an object through physical contact with a sensing device.[1] Nowadays, a number of techniques are available for the transduction of interface contact pressure or force between objects, which are described in several literature reviews on tactile sensing research. Most of these devices originate from biomedical and humanoid robot applications.[1-5] Among all possible working principles, only few promising technologies are capable to fulfill the requirement of these sensors for various applications. Currently, the most frequently used are the capacitive and resistive sensors. The former is based on the change of capacitance between two parallel plates due to a deformation induced externally, whilst the latter is based on the resistance change of a piezoresistive layer when a deformation is applied.

Moreover, biomedical and robotic tactile sensors usually need to be flexible and adapt to the curvature of the hosting structures, and stretchable to cover joint and moving parts in order to measure the interaction force correctly.[6]

In previous experimental works we have reported various novel piezoresistive composites based on nanostructured metal fillers dispersed in a silicone matrix as functional material for tactile devices, where the achieved wide variation of piezoresistance was ascribed to the quantum tunneling conduction induced by the spiky particles covered by nanometric tips.[7,8] In the un-deformed condition the composite material shows an insulating behavior, while after applying a strain the electrical conductivity exponentially increases.[9,10] In these composites, conductive particles are separated from each other by a thin gap of insulating polymer representing the tunneling barrier. By applying a deformation to the sample, the thickness of the tunneling barrier is reduced, thus increasing the probability of tunneling phenomena and resulting in a huge reduction of the bulk electrical resistance.

Concerning the electrodes deposition technique, the literature reports several technologies and materials for flexible composites and rubber-based functional materials.[11-13] Direct metal deposition allows the fabrication of very conductive electrodes and it ensures very low contact resistance values, yet it suffers from a stiffness mismatch between the metallic electrodes and the polymer composite functional material. The differences in Young module and elongation at brake could induce the formation of a crack in the stiff electrode material during the stretching or bending of the device, consequently compromising electrical conduction. Moreover, the bonding force between the polymeric-based functional material and the metalized electrode film might result too weak to ensure a good adhesion, and peeling off / detachment effects may occur.[14-16] Due to an extremely high metal to polymer ratio, resulting in different surface and dielectric properties of the composite, known plasma conditions are not suitable to allow control of the spreading. To overcome these problems, this work reports the optimization of direct printing of polymeric electrodes on the surface of plasma-treated composite materials.

Inkjet printing (IjP) is a versatile manufacturing technique for the direct deposition of electrical contacts on a variety of substrates.[17] Several reviews on new applications of IjP technology report the use of conductive inks based on metallic nanoparticles, which can either be dispersed in a carrier, or generated in-situ by chemical reaction.[18] Nanoparticle-based inks normally feature extremely high conductivities but require rather high temperatures for sinterization.[19,20] Another

possibility is represented by polymeric inks filled with graphene, but these are not yet suitable for practical applications as they feature high resistivities or require anyway thermal sintering.[21,22] More recently, inks based on conductive polymers were also developed.[23] These are predominantly indicated for the fabrication of electrical patterns on substrates that cannot undergo thermal treatments, which are required in most inks based on metallic nanoparticles. In particular, inks based on poly(3,4-ethylenedioxythiophene) poly(styrenesulfonate) (PEDOT:PSS) were developed for this purpose because of the good solubility and ease of processing, and can be used as transparent, conductive coatings with high ductility.[24]

The adhesion of the printed drops to the substrate is influenced not only by the rheological characteristics of the printed fluid, which can be adjusted before and during the printing process, but also by the physical and chemical properties of the substrate surface. PEDOT:PSS patterns show poor adhesion properties and imprecise geometry reproduction when printed on highly hydrophobic substrates such as polydimethylsiloxane (PDMS). Liquid spread is influenced by fluid properties such as surface tension and viscosity, and by the relative surface energy and roughness of the substrate. It is therefore possible to limit and tune the ink drops spread by carefully modifying the surface energy of the substrate.[25] Moreover, surface morphology and modification can impact heavily on the way in which sessile drops deposit on a substrate, by enhancing or limiting their coalescence.[26]

Surface modification techniques, such as wet chemical treatment, low pressure plasma treatment, and UV irradiation have been widely applied to different substrates to enhance their adhesion properties and their applicability in functionalization processes in general.[27,28] Among them, low pressure plasma treatments have been strongly exploited because they have proven to be an effective way to modify the surface of polymers. Many properties and functionalities can be obtained by plasma treatment, depending on the application: plasma can be used to tailor the surface wettability, improve barrier characteristics, adhesion, dye-ability, printability, oleophobicity.[29] Chemical surface modification is initiated by the radical reaction of plasma species and the most external layers of the substrate surface, which occurs without modification of the bulk properties. In comparison to traditional low pressure plasma treatments, requiring high vacuum equipment, or wet chemical treatments, which often involve the use of non-environmentally friendly chemicals and methods, plasmas operating at atmospheric pressure (APPs) offer an interesting alternative because of in-line process capabilities, relatively low costs, possible high throughput and low requirements on personal and environmental safety. In addition, non-thermal APPs usually work at temperatures in the range of 50–200°C, so they can be safely employed for polymer modification. Several types of APPs operating in the regime of a non-thermodynamic equilibrium exist. Typical APP systems are corona discharges and Dielectric Barrier Discharges (DBD).[29,30] With the purpose of achieving a uniform surface treatment, plasmas homogeneous in time and space are desirable, although they are not always achievable with traditional corona discharges and DBDs. For instance, large plasmas were obtained using a series of individual discharges to form a larger array, or using the DBD homogeneous mode, also called Atmospheric Pressure Glow discharge (APG).[31,32] This mode is characterized by the absence of streamers and by the presence of a uniform glow which is highly reminiscent of a low pressure glow discharge. Its selective characteristics can be adapted to a variety of treatments for various shapes and type of substrates.

In this work, an APP was tested for the modification of the surface of highly hydrophobic PDMS-based composite materials, containing a high volume fraction of metallic particles, whose presence causes a strong interaction of the material with the APP metallic electrodes. This procedure allowed the optimization of the surface properties of the composites for the deposition of PEDOT-PSS electrodes by inkjet printing.

Experimental

Piezoresistive Nanocomposite Preparation.

The piezoresistive composite material was fabricated from bi-component polydimethylsiloxane (Dow Corning Corporation - SYLGARD 184) and nanostructured copper particles (POMETON Ltd. - LT10) presenting spiky tips on the surface with a technological process flow already described in previous works.[7,8] The powder was dispersed in the PDMS base and then, after the addition of the PDMS curing agent, the blend was gently mixed in order to prevent the tip smoothing and disruption. The resulting paste was poured in PMMA moulds, outgassed in vacuum and cured in oven at 70ºC for three hours.

A sketch of the whole technological process starting from the preparation of the piezoresistive material up to the electrodes deposition is presented in Figure 1.

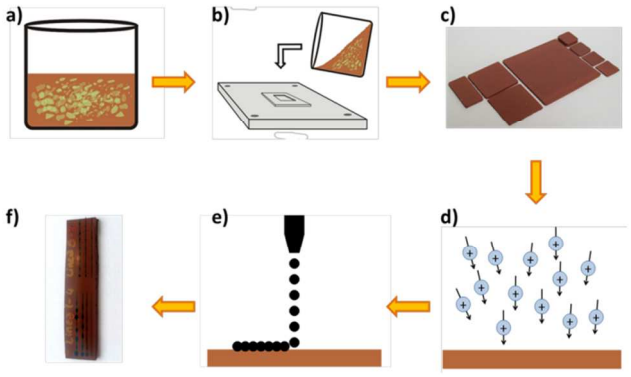

Figure 1. Sketch of the technological process for the preparation of the piezoresistive composite. a) Component mixing, b) composite pouring, c) demolding after curing step, d) plasma treatment, e) inkjet printing and f) composite with PEDOT:PSS lines.

Atmospheric Plasma System.

The samples surfaces were treated using a DBD APP system (manufactured by ARIOLI S.p.A., Italy). The plasma discharge was lit applying a RF bias, in the 30-50 kHz frequency range, between a metallic planar electrode, covered by a polymeric dielectric layer, and a plasma process tool. Two different types of plasma process tools were used, the first consisting of a set of stainless steel cylindrical electrodes of 30 cm in length and the second consisting of a set of ceramic electrodes of square cross section of the same length (detailed in Figure 2a). The power applied to the plasma process tool was in the range 400-550 W and 500-1100 W for the stainless steel and the ceramic electrodes, respectively. Using the stainless steel tool, the maximum RF power that could be applied was limited by the interference between metallic particles dispersed in the PDMS sample and the metal electrodes. This effect was reduced using

the ceramic tool, allowing the application of high RF power to the samples. An Ar flow of 10 l/min was injected near the electrodes in order to displace the air and fill with Ar gas the plasma volume, thus allowing a better control of the process atmosphere and improving the homogeneity of the plasma streamers. The treatments were applied moving the plasma process tool, at a speed of 83 mm/s, in direction parallel to the samples, which were located on the planar dielectric layer. The vertical distance between the planar dielectric layer and the plasma process tool was varied in the range 1.8-2.3 mm, depending on the sample thickness. Due to the possibility of moving the multi-electrodes tool back and forth, different numbers of passes have been tested. The energy per unit area applied to the samples, calculated as P n / (v l) where P is the power, n the number of passes, v the speed and l the electrodes length, resulted in the range 80-110 kJ m^{-2} for the metal tool and 100-220 kJ m^{-2} for the ceramic tool.

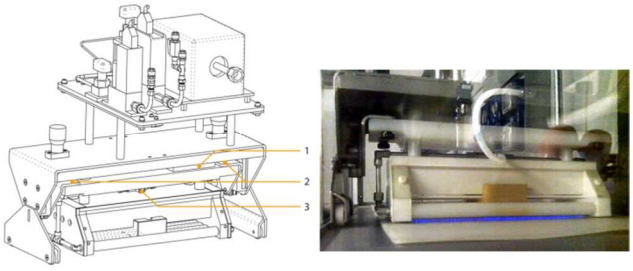

Figure 2. a) detail scheme of the ceramic multi-electrode tool, where the high voltage connector (1), the insulation (2) and the tube used to inject vaporized species (3) are evidenced; b) picture of the active APP Ar glowing discharge by ceramic multi-electrode.

Contact Angle Measurements.

The effect of the surface plasma treatment has been investigated by means of Optical Contact Angle (OCA) measurements, with an OCAH 200 instrument (DataPhysics Instruments GmbH), equipped with CCD camera and automatic dosing system of the liquid. Deionized water MilliQ grade (H_2O) and diiodomethane (CH_2I_2 – Sigma Aldrich) were used as liquids (droplet volume = 1.5 µl), for the analysis according to sessile droplet method in static mode. Datasets of liquid surface tension and dispersive/polar contributions for water and diiodomethane are γ_{H2O}= 72.8 mN where γ^d = 21.8 mN/m and γ^p =51.0 mN/m and γ_{CH2I2} = 50.8 mN/m where γ^d = 48.5 mN/m and γ^p = 2.3 mN/m.[33,34] Drop profiles were fitted through the Young–Laplace method, and contact angles between fitted function and base line were calculated by the SCA20 software.[35] Standard deviation was calculated for each kind of sample on a data set of at least three droplets for each liquid. Surface free energy of both bare and plasma treated surfaces was determined through the Owens and Wendt method [36], according to details reported Supporting Information.
In order to calculate these parameters, the contact angle of at least two liquids on the unknown solid was determined (water and diiodomethane in the present case).

Inkjet Printing Deposition of Electrodes.

PEDOT:PSS commercial ink (CleviosTM from Heraeus Precious Metals GmbH, Germany) was used as received. The ink was inserted into a 3 ml reservoir and loaded to the IjP system (JETLAB 4-XL from Microfab, US). The system is equipped with independent heaters for the printing nozzle and the substrate. Printing tests were achieved through piezoelectric nozzles made in quartz, with diameter of 80 µm, with a vibration frequency set to 500 Hz. The dimension and speed of ink drops were controlled by a horizontal camera located onto the x-y stage for direct drop observation. Jetting parameters were set as follows, using an asymmetrical pulse: first rise time 3 µs, dwell time 8 µs, fall time 8 µs, echo time 15 µs, second rise time 3 µs, idle voltage 3 V, dwell voltage 35 V, echo voltage -35 V. The nozzle was heated to a temperature of 40°C in order to obtain the correct value of ink viscosity suitable for printing. Tracks with length of 20 mm were printed, varying the resolution of the spotted ink droplets from 75 to 400 points per line (ppl), and varying the number of subsequent passes between 1 and 10, and let dry in air.

Morphological Characterizations.

Morphological characterization of untreated and plasma treated surface of PDMS/Cu composites was performed by means of Field Effect Scanning Electron Microscopy (FESEM, ZEISS Dual Beam Auriga). Track widths were measured and track morphology determined under different printing parameter settings and various surface treatment using conventional optical microscopy (ZEISS AXIO). Optical microscope image analysis was performed using proprietary routines written in Matlab® M-script.

Electrical Characterization.

Functional characterization was performed on printed tracks using standard 2-point micro-contact setup at room temperature, in DC regime, using a Keithley 2635A multimeter.[37, 38] Each sample has been measured in the same conditions three times, in order to get sufficient data and process experimental points, computing the average and standard deviation.

Results and Discussion

Contact Angle Analysis.

The surface of bare Cu micro particles-PDMS composite samples, 1 mm thick, has been treated by means of an atmospheric pressure plasma customized system, in order to enhance controlled spreading of ink droplets and promote their coalescence. This was expected to improve the surface adhesion of the printed ink and ensure the continuity of conductivity for the device. Several process parameters permutations have been tested for both types of electrode (metallic and ceramic), including RF Power and number of passes, in order to achieve a homogeneous discharge, approaching the condition of an atmospheric glow discharge on the exposed area and a quasi-permanent effect of treatment. Table 1 reports Contact Angle analysis data (contact angle of both selected liquids and surface free energy, together with dispersive and polar contribution) for the optimized process described in the experimental section, for the maximum applied RF Power (1100 W) and 5 passes, by employing the ceramic multi-electrode tool and by measuring the samples before and after plasma process, both soon after the treatment and after a 2 h aging.

Table 1. Water and diiodomethane Optical Contact Angle (OCA) values and Surface Energy (SE) values divided in the polar and dispersive contributions of untreated, treated and aged Cu

microparticles-PDMS composites.

Samples	OCA PEDOT [°]	OCA H_2O [°]	OCA CH_2I_2 [°]	Surface Energy [mN/m]	Dispersive Component [mN/m]	Polar Component [mN/m]
Cu-PDMS	50±1	122±4	90±1	13.0	13.0	0.0
Cu-PDMS after Ar-plasma	22±1	16±1	45±2	70.0	22.2	47.8
Cu-PDMS after 2h ageing post-plasma	28±1	29±4	49±1	64.0	21.4	42.6

Cu-PDMS composite shows the typical water contact angle of bare PDMS, about 120°, suggesting that the metallic microparticles are confined in the bulk and do not affect surface properties. Moreover, the surface energy of the sample is very low (13 mN/m), due also to the scarce interaction with diiodomethane, as reported for pure PDMS in [39]. The polar component of diiodomethane surface tension cannot be ignored, so preventing its spreading on the highly non-polar PDMS surface. A higher wettability could be reached only with non-polar liquids such as hexadecane (polar component of surface tension is equal to 0 mN/m). The samples measured just after the plasma process show an abrupt decrease of water contact angle (down to 16°) and an increase of surface energy (up to 70 mN/m) typical of highly hydrophilic substrates. Both polar and dispersive components result strongly modified by the treatment, owing to strong oxidation of the surface as Ar plasma is activated in atmospheric air (the former), and structural changes in PDMS polymeric surface chains (the latter), ascribable to physical ablation performed by the discharge.[40] The increased roughness and thereby surface area, even though not visible to the naked eye, could improve the wettability by a quite non-polar liquid such as diiodomethane, if compared with the poor spreading obtained on the untreated smooth substrate.[41]

Since surface energy may not be the only reason for improved adhesion of the PEDOT ink after solvent evaporation, although it does certainly affect its wettability when the ink is still in the liquid phase, we also performed en evaluation of the surface roughness before the plasma processing, after the treatment and on aged samples. The images shown in Figure 3 were used for the roughness evaluation, adapting them to run on a Matlab® routine previously developed to analyze particles and grains.[42-44] Results, reported in Table 2, indicate that roughness is doubled by the plasma treatment and is not affected by aging, since it produces a physical modification of the composite.

Table 2. Roughness of untreated, treated and aged Cu microparticles-PDMS composites, estimated according to a numerical algorithm based on FESEM images (Figure 3).

	Cu-PDMS	Cu-PDMS after Ar-plasma	Cu-PDMS after 2h ageing post-plasma
Roughness [nm]	383±300	716±120	716±120

The permanence of the effect of the plasma treatment was studied by performing the aging experiments. The contact angle analyses were repeated on the samples left for 2h in open air. Table 1 shows that contact angles measured with standard liquids are slightly affected by aging, resulting in a little decrease of surface energy (64 mN/m). Among the several attempted processes, only one (ceramic multi-electrode tool, power =1100 W, 5 passes) allowed to achieve a non-trivial goal, such as a quite good compromise among surface spreading enhancement, limited advantageous modification of surface roughness and permanence of produced effects for a time long enough to allow the inkjet printing without the need of a multi-step implant. Considering that PEDOT:PSS ink has a surface tension of 62 mN/m (reported in CleviosTM datasheet), a contact angle similar to water is expected.

It is worth noticing that the ink shows a lower contact angle than water on the bare Cu-PDMS composite, due to the presence of organic components that make it more compatible with the hydrophobic untreated polymeric surface. As expected, the plasma treatment produced a similar effect to both water and ink, thus it can be inferred that the treatment acted on the aqueous component of the ink. The PEDOT:PSS wetting of polymeric/metallic composite can be considered stable within 2h after the plasma modification. A longer storage time is known to lead to the recovery of surface hydrophobic properties of pristine PDMS, even after an oxygen plasma treatment under vacuum.[45] In the following paragraphs, it is demonstrated that the decrease of about 20° in contact angle, i.e. 6 mN/m in Surface Energy, allows to achieve the desirable spreading of ink drops, promoting the liquid coalescence and its adhesion helped by the improved wettability of the surface. The fulfilment of these requirements is needed for the production of functional printed electrodes.

The best results of surface modification using the metallic electrode tool have been obtained with the 4 passes process at 550 W. The values of contact angle for water and diiodomethane are comparable. However, the use of this setup lead to a less homogenous discharge due to the formation of separated arcs. This possibly caused the motion of Cu microparticle clusters towards the surface, which resulted in removal of material and creation of holes and cracks on the surface of the composite. The result of this plasma treatment was clearly observed by FESEM analysis and a topography view is shown in Figure 3a. This phenomenon induces a modification of bulk composition, in terms of micro-particles distribution, that may negatively affect the piezoelectric device performance inducing the formation of electrically non-homogeneous clusters on the sample surface. These phenomena are considerably reduced when using the ceramic tool, which limits particles removal and surface damage, as visible in Figure 3b and 3c.

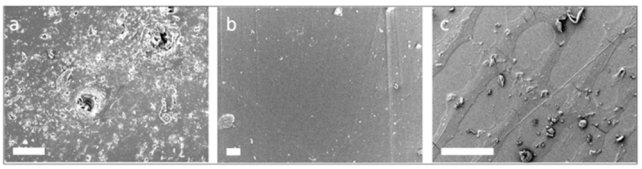

Figure 3. FESEM analysis of the composite surface after plasma

treatment with a) metallic tool at 550 W (a deep damage of the surface, consistent with the appearance of erosion, is visible) and b,c) ceramic tool at 1100 W. In c) the inkjet printed PEDOT:PSS lines are visible. The scale bars correspond to 20 µm.

Analysis of Inkjet Printed Electrodes on top of the composite.

Figure 4 shows a chromatically enhanced optical microscope image collection of PEDOT:PSS patterns printed on PDMS/Cu composites before and after plasma treatment performed with the metallic tool. In particular, an array of straight lines is analyzed, composed by a number of droplets with density comprised in the range 100 – 400 points per line (ppl). The analysis of untreated surfaces confirms the poor wettability of the bare composite surface. On the other hand, it is possible to notice that a bulging is induced on the liquid ink printed on the treated surfaces.[46] This consists in a hydrodynamic instability producing regions that accumulate liquid subtracting it from other depleted regions, where the printed line is thinned and in some cases even interrupted. This phenomenon is more evident for the most energetic treatment (550 W for 4 passes) and for the pattern printed at high resolution (400 ppl).

The bulging phenomenon may be controllable when the APP treatment is performed by multi-electrode ceramic tool, with plasma powers up to 1100 W. In the next paragraph an operative procedure to correlate an engineering parameter (plasma hardness, defined further in the text) with post-printing features, such as good adhesion, bulging, etc. will be presented. We will see that a low hardness plasma treatment leads to a very low wetting, while a high one leads to high bulging.

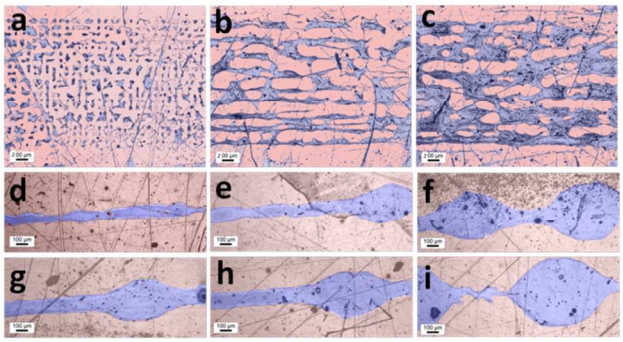

Figure 4. Collection of optical microscope images showing the surface of inkjet-printed tracks on top of PDMS/Cu composites. First row: untreated surfaces, 3 (a), 5 (b) and 10 (c) passes, printed tracks of nominal width 1 mm. Second row: printed tracks of nominal width 100 µm, after APP treatment with metallic tool at 400 W 3 passes, at 100 (d), 200 (e) and 400 (f) ppl. Third row: printed tracks of nominal width 100 µm, after APP treatment with metallic tool at 550 W 4 passes, at 100 (g), 200 (h) and 400 (i) ppl.

The information content of each microscope image has been extracted by means of numerically assisted image analysis (IA) procedure, as evidenced in the composite Figure 5, where the first row sketches an example of processing of a sample image, while the second row contains data extracted from all the images taken on samples treated at 400 W, metallic electrode. In particular, each histogram frame has been adjusted before conversion from RGB to 8-bit grayscale, further posterized to a 2-bit valued B/W map (Figure 5b); then a filter to detect image edges has been applied, based on Sobel Gaussian computation; the resulting edge image (Figure 5c), has been imported in the Matlab® environment for statistical analysis. Each edge position, both the upper and lower, has been stored in a sequence of vectors (Figure 5d) and further studied, extracting its mean edge position, standard deviation and so on. Each edge pixel, identified by a couple of values corresponding to its (x,y) coordinates, has been used to populate a statistic, limited to the y-position. The bin center is hence the average y-position of the edge (zero) and the relative frequency is the number of pixel having a certain position over the total number of edge pixels (Figure 5e). It is clear that a straight edge would result in a monodisperse statistics, with a very narrow peak centered at the mean value. Conversely, a bulging edge would result in a very disperse and broad peak, still centered at the mean value. When the periodicity of the bulging is such that in the same frame we can identify more than one ink circular area, then a double peak broad distribution is found. For completeness, the experimental cumulative distribution is also given (Figure 5f), showing perhaps the strongest evidence of the effects induced on the adhesion between ink and substrate by printing parameters, in this case the droplet density.

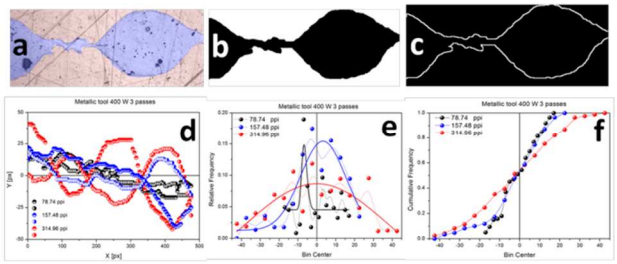

Figure 5. First row: Image Analysis procedure used to transform the optical microscope image of a printed track (a) into a 2-bit valued B/W map (b) and finally to a 2-bit valued map with edge evidenced (c). Second row: upper and lower profiles, as numerically extracted from optical microscope imaging of samples treated with metallic tool at 400W, under different printing conditions (d); relative frequency plot of the edge statistics, obtained by normal Gaussian profile fitting (e); cumulative frequency plot of the edge statistics (f).

Using the profiles represented in Figure 5d we have performed the following statistical analysis, shown in the relative frequency plot of Figure 5e. Three different printing densities (indicated as points per inch, ppi) result in three very different situations, where the peak broadening is consistent with the occurrence of bulging from a straight line. On the x-axis, bin center is given in pixels; it is straightforward to see that increasing the IjP density, the printed area broadens and the excursion covered on the x-axis is greater. A slight asymmetry of the frequency profiles (horizontal shift with respect to zero) is due to misalignment of the line axis with respect to microscope frame axis, but this un-compensated effect is not affecting the following discussion. The cumulative frequency plot of Figure 5f compares the almost

perfectly linear statistics of the sample printed at low density (straight line) with the other cases at higher printing density, featuring a smoother distribution.

The results of the IA procedure are graphically presented in Figure 6, showing the efficacy of our numerical procedure in smartly classifying different plasma treatments. Figure 6a represents the bulging broadness as a function of APP hardness, giving also information on effective ink volumes as a color scale (goal function). The plasma treatment hardness (engineering parameter) is defined as the APP power multiplied by the number of passes over the time elapsed since the treatment before IjP and the engineering volume is defined as the track density multiplied by the number of printing passes. Figure 6a demonstrates that the phase space can be experimentally explored almost entirely by changing process parameters. A low hardness plasma treatment leads a low volume IjP sample to a very low broadness/wetting of the surface, while a high hardness plasma treatment leads almost every volume to high bulging broadness.

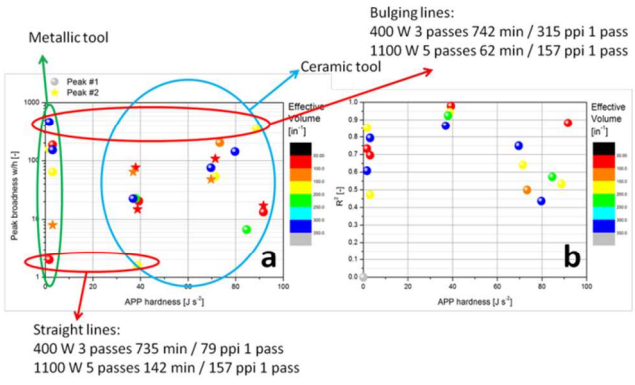

Figure 6. Peak #1 and peak #2 broadness (a) and R2 (b) as a function of the APP hardness, where each sample engineering volume has been represented in color scale; all experimental samples are here reported.

Figure 6b represents the Gaussian fit R2 to the relative probability (Figure 5) as a function of APP hardness and effective volume: the higher this factor, the better the Gaussian fit; it should be noted that there is no theory behind the choice of the Gaussian distribution, other than its simplicity. When a simple criterion is applied with success, the corresponding process is also easily controllable. Depending on the relative probability distribution, single Gaussian or double Gaussian fits were performed. Both hard and soft APP treatments produce results whose statistics are not well represented by the simple Gaussian model, while mild treatments, those around 40 Js^{-2}, are better described. The fill factor is defined as the number of pixels containing ink over the total number of pixels belonging to the area to be printed. This number has been computed only for the samples having a defined area to be printed (untreated substrate), while for other samples, where line broadness results directly from droplet density and is not user-defined, we have given a fixed value of 1. The peak broadness is computed as the Gaussian fit peak width over its height. One of the key objectives of this study is finding an effective experimental procedure to limit ink consumption, so the engineering volume should be as low as possible and the fill factor should be 1. We have observed that even a high number of passes (10) is not enough to approach these values, hence the necessity of an APP treatment. The fit is also useful for a quick evaluation of the fabrication procedure, since its broadness should approach zero for perfectly straight lines without printing defects, while lines evidencing bulging would result in a broader peak and in a double peak distribution.

Functional Characterization.

The electrical characteristics of printed tracks were measured on selected portions of the composite. Figure 7a shows a typical response in the low voltage regime: by contacting the composite sensing skin directly with tungsten micro-probes, the overall current flowing through the sample is low, even though the experimental error is kept always well below 10% (red circles). When contacts are placed on the PEDOT:PSS printed tracks, the current flowing through the system is higher – more than doubled at positive potentials – but also the standard deviation is increased, reaching up to 25% at positive potentials. This may be also due to plasma induced surface damage (Fig. 3a).

This type of material is normally used under low voltage conditions, as it is intended to be coupled to standard electronic devices (5 V) and low power energy sources [8]. However, high electric field conditions were already used to induce electric ageing of nanocomposite samples in similar systems.[47] Therefore, the high voltage regime was also investigated, to potentially induce electromigration and exclude drifts in its response. Figure 7b shows that in the high voltage regime our system after PEDOT:PSS printing saturates and the standard deviation may be as high as 100%. The saturation seen in the response tells us that there is no threshold for electromigration and that this noise is entirely due to instability toward high charge.

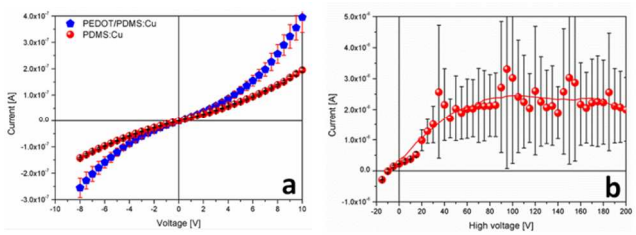

Figure 7. Two point IV curves acquired in the low (a) and high (b) voltage regime from the top surface of a piezoresistive Cu:PDMS sensor before and after (a), after (b) the deposition of inkjet printed flexible polymeric electrodes.

Conclusions

The optimization of an original process, based on atmospheric pressure plasma treatment, for improving the compatibility of an organic intrinsically conductive polymer with the hydrophobic surface of a composite material with extremely high metal to polymer ratio was described. In particular, a composite piezoresistive artificial skin based on a matrix of PDMS and a dispersion of copper particles was tested. This process requires the use of an atmospheric pressure plasma treatment, which was tested using both metallic and ceramic RF electrode tools, resulting in several experimental values of damage on the surface of the polymer, contact angles, adhesion and spreading of the ink. An novel procedure to quantify the drop spreading was also developed, based on optical microscope image analysis and numerical routine used to extrapolate quantitative data from the bulging degree of the printed track profile. By quantifying also the energy transferred to the substrate by means of the plasma treatment, it was possible to create a phase diagram which was

useful to understand and smartly classify the optimal conditions for the improvement of compatibility.

Electrical characterization was performed on untreated / treated samples after inkjet printing of electrodes, evidencing an improved signal and the absence of electromigration.

Notes and references

[a] Center for Space Human Robotics, Istituto Italiano di Tecnologia, Corso Trento 21, 10129 Torino, Italy, E-mail: alessandro.chiolerio@iit.it.

[b] Applied Science and Technology Department, Politecnico di Torino, Corso Duca degli Abruzzi 24, 10129 Torino, Italy.

Electronic Supplementary Information (ESI) available: [details of any supplementary information available should be included here]. See DOI: 10.1039/b000000x/

[1] Lee, M. H. Tactile sensing: new directions, new challenges. International Journal of Robotics Research 2000, 19(7), 636.

[2] Tiwana, M.I.; Redmond, S.J.; Lovell, N.H. A review of tactile sensing technologies with applications in biomedical engineering. Sensors and Actuators A: Physical 2012, 179(0), 17.

[3] Maheshwari, V.; Saraf, R. Tactile Devices To Sense Touch on a Par with a Human Finger. Angewandte Chemie International Edition 2008, 47(41), 7808.

[4] Yousef, H.; Boukallel, M.; Althoefer, K. Tactile sensing for dexterous in-hand manipulation in robotics—A review. Sensors and Actuators A: Physical 2011, 167(2), 171.

[5] Bar, C.A. Evaluation of cushions using dynamic pressure measurement. Prosthet. Orthot. Int. 1991, 15(3), 232-40.

[6] Duchaine, V.; Lauzier, N.; Baril, M.; Lacasse, M.-A.; Gosselin, C. A Flexible Robot Skin for Safe Physical Human Robot Interaction. IEEE International Conference on Robotics and Automation Kobe, Japan. 2009, 3676.

[7] Stassi, S.; Canavese, G. Spiky nanostructured metal particles as filler of polymeric composites showing tunable electrical conductivity. Journal of Polymer Science Part B: Polymer Physics 2012, 50(14), 984.

[8] Tommasi, T.; Chiolerio, A.; Crepaldi, M.; Demarchi, D. A microbial fuel cell powering an all-digital piezoresistive wireless sensor system. Microsystem Technologies 2014, 20, 1023-1033.

[9] Bloor, D.; Donnelly, K.; Hands, P. J.; Laughlin, P.; Lussey, D. A metal–polymer composite with unusual properties. J. Phys. D: Appl. Phys. 2005, 38, 2851.

[10] Canavese, G.; Lombardi, M.; Stassi, S.; Pirri, C. F. Comprehensive characterization of large piezoresistive variation of Ni-PDMS composites. Applied Mechanics and Materials 2012, 110, 1336.

[11] Patel, J. N.; Kaminska, B.; Gray, B. L.; Gates, B. D. A Sacrificial SU-8 Mask for Direct Metallization on PDMS. J. Micromech. Microeng. 2009, 19, 115014.

[12] Buselli, E.; Smith, A.M.; Grover, L.M.; Levi, A.; Allman, R.; Mattoli, V.; Menciassi, A.; Beccai, L. Development and characterization of a bio-hybrid skin-like stretchable electrode. Microelectronic Engineering 2011, 88, 1676–1680.

[13] Chang, M.P.; Maharbiz, M.M. Electrostatically-driven elastomer components for user-reconfigurable high density microfluidics. Lab Chip. 2009, May 7; 9, 1274-81.

[14] Yu, C.; Wang, Z.; Yu, H.; Jiang, H. A Stretchable Temperature Sensor Based on Elastically Buckled Thin Film Devices on Elastomeric Substrates. Appl. Phys. Lett. 2009, 95, 141912.

[15] Delcorte, A.; Befahy, S.; Poleunis, C.; Troosters, M.; Bertrand, P. Adhesion improvement for metallized silicone films. Adhesion Aspects of Thin Films 2004, Vol. 2, 1–12.

[16] Sim, G.D.; Won, S.; Jin, C.; Park, I.; Lee, S. B.; Vlassak, J. J. Improving the stretchability of as-deposited Ag coatings on poly-ethylene-terephthalate substrates through use of an acrylic primer. J. Appl. Phys. 2011, 109, 073511.

[17] Klauk, H. Plastic electronics: Remotely powered by printing. Nat. Mater. 2007, 6, 397.

[18] Singh, M.; Haverinen, H.M.; Dhagat, P.; Jabbour, E.G. Inkjet Printing—Process and Its Applications. Adv. Mat. 2010, 22, 673.

[19] Chiolerio, A.; Maccioni, G.; Martino, P.; Cotto, M.; Pandolfi, P.; Rivolo, P.; Ferrero, S.; Scaltrito, L. Inkjet printing and low power laser annealing of silver nanoparticle traces for the realization of low resistivity lines for flexible electronics. Microelectronic Engineering 2011, 88, 2481-2483.

[20] Chiolerio, A.; Cotto, M.; Pandolfi, P.; Martino, P.; Camarchia, V.; Pirola, M.; Ghione, G. Ag nanoparticle-based inkjet printed planar transmission lines for RF and microwave applications: Considerations on ink composition, nanoparticle size distribution and sintering time. Microelectronic Engineering 2012, 97, 8-15.

[21] Giardi, R.; Porro, S.; Chiolerio, A.; Celasco, E.; Sangermano, M. Inkjet printed acrylic formulations based on UV-reduced graphene oxide nanocomposites. J. Mater. Sci. 2013, 48, 1249-1255.

[22] Secor, E.B.; Prabhumirashi, P.L.; Puntambekar, K.; Geier, M.L.; Hersam, M.C. Inkjet Printing of High Conductivity, Flexible Graphene Patterns. J. Phys. Chem. Lett. 2013, 4, 1347-1351.

[23] De Gans, B.J.; Duineveld, P.C.; Schubert, U.S. Inkjet Printing of Polymers: State of the Art and Future Developments. Adv. Mater. 2004, 16, 203.

[24] Xiong, Z.; Liu, C. Optimization of inkjet printed PEDOT:PSS thin films through annealing processes. Organic Electronics 2012, 13, 1532.

[25] Ely, F.; Avellaneda, C.O.; Molina, C.; Paredez, P.; Nogueira, V.C.; Santos, T.E.A.; Mammana, V.P.; Brug, J.; Gibson, G.; Zhao, L. Patterning quality control of inkjet printed PEDOT:PSS films by wetting properties. Synthetic Metals 2011,161, 2129-2134.

[26] Graham, P. J.; Farhangi, M. M.; Dolatabadi, A. Dynamics of droplet coalescence in response to increasing hydrophobicity. Phys. Fluids 2012, 24, 112105-1-112105-20.

[27] Lee, K. W.; Kowalczyk, S. P.; Shaw, J. M. Surface modification of BPDA-PDA polyimide. Langmuir 1991, 7, 2450-2453.

[28] Zhang, J. Y.; Esrom, H.; Kogelschartz, U.; Eming, G. Modification of polymers with UV excimer Radiation form lasers and lamps. J. Adhes. Sci. Technol. 1994, 8, 1179-1210.

[29] Park, J. B.; Oh, J. S.; Gil, E. L.; Kyoung, S. J.; Lim, J. T.; Yeoma, G. Y. Polyimide Surface Treatment by Atmospheric Pressure Plasma for Metal Adhesion. Journal of The Electrochemical Society 2010, 157, 12, D614-D619.

[30] Noeske, M.; Degenhardt, J.; Strudthoff, S.; Lommatzsch, U. Plasma jet treatment of five polymers at atmospheric pressure: Surface modifications and the relevance for adhesion. International Journal of Adhesion & Adhesives 2003, 24, 171-177.

[31] Kunhardt, E. Generation of large – volume, atmospheric- pressure nonequilibrium plasmas. IEEE Trans. Plasma Sci. 2000, 28(1), 189-200.

[32] Kanazawa, S.; Kogoma, M.; Moriwaki, T.; Okzaki, S. Stable glow plasma at atmospheric pressure. J. Phys. D: Appl. Phys. 1988, 21, 838-840.

[33] Ström, G.; Fredriksson, M.; Stenius, P. Contact Angles, Work of Adhesion, and Interfacial Tensions at a Dissolving Hydrocarbon Surface. J. Colloid Interf. Sci. 1987, 119 No. 2, 352-361.

[34] Fowkes, F.M. Attractive Forces at Interfaces. Ind. Eng. Chemistry 1964, 56 No. 12, 40-52, Table VIII.

[35] Hansen, F.K. Surface tension by image analysis fast and automatic measurements of pendant and sessile drops and bubbles. Journal of Colloid and Interface Science 1993, 160, 209-217.

[36] Owens, D. K.; Wendt, R. C. Estimation of the surface free energy of polymers. J. Appl. Polym. Sci. 1969, 13, 1741-1747.

[37] Bocchini, S.; Chiolerio, A.; Porro, S.; Accardo, D.; Garino, N.; Bejtka, K.; Perrone D.; Pirri, C.F. Synthesis of polyaniline-based inks, doping thereof and test device printing towards electronic applications. J. Mater. Chem. C 2013, 1, 5101.

[38] Chiolerio, A.; Bocchini, S.; Porro, S. Inkjet printed negative supercapacitors: synthesis of polyaniline-based inks, doping agent effect, and advanced electronic devices applications. Adv. Funct. Mater. 2014, 24, 3375-3383.

[39] Lamberti, A.; Quaglio, M.; Sacco, A.; Cocuzza, M.; Pirri, C.F. Surface energy tailoring of glass by contact printed PDMS. Applied Surface Science 2012, 258, 9427– 9431.

[40] Kim, H.T.; Jeong, O. C. PDMS surface modification using atmospheric pressure plasma. Microelectronic Engineering 2011, 88, 2281–2285.

[41] Ramiasa, M.; Ralston, J.; Fetzer, R.; Sedev, R. The influence of topography on dynamic wetting. Adv. Colloid Interface Sci. 2013, in press, DOI: 10.1016/j.cis.2013.04.005.

[42] Chiolerio, A.; Cotto, M.; Pandolfi, P.; Martino, P.; Camarchia, V.; Pirola, M.; Ghione, G. Ag nanoparticle-based inkjet printed planar transmission lines for RF and microwave applications: considerations on ink composition, nanoparticle size distribution and sintering time. Microelectron. Eng. 2012, 97, 8-15.

[43] Virga, A.; Rivolo, P.; Descrovi, E.; Chiolerio, A.; Digregorio, G.; Frascella, F.; Soster, M.; Bussolino, F.; Marchiò, S.; Geobaldo, F.; Giorgis, F. SERS active Ag nanoparticles in mesoporous silicon: detection of organic molecules and peptide-antibody assays. J. Raman Spectrosc. 2012, 43, 730-736.

[44] Chiolerio, A.; Virga, A.; Pandolfi, P.; Martino, P.; Rivolo, P.; Geobaldo, F.; Giorgis, F. Direct patterning of silver particles on porous silicon by inkjet printing of a silver salt via in-situ reduction. Nanoscale Res. Lett. 2012, 7, 502.

[45] Bodas, D.; Khan-Malek, C. Hydrophilization and hydrophobic recovery of PDMS by oxygen plasma and chemical treatment—An SEM investigation. Sensors and Actuators B 2007, 123, 368–373.

[46] Soltman, D.; Subramanian, V. Inkjet-Printed Line Morphologies and Temperature Control of the Coffee Ring Effect. Langmuir 2008, 24, 2224-2231.

[47] Chiolerio, A.; Vescovo, L.; Sangermano, M. Conductive UV-cured acrylic inks for resistor fabrication: models for their electrical properties. Macromol. Chem. Phys. 2010, 211, 2008-2016.